

High critical current density and improved irreversibility field in bulk MgB₂ made by a scaleable, nanoparticle addition route

J. Wang, Y. Bugoslavsky, A. Berenov, L. Cowey, A. D. Caplin, L. F. Cohen, and J. L. MacManus Driscoll^{a)}

Centre for High Temperature Superconductivity, Imperial College, Prince Consort Road, London SW7 2AZ, United Kingdom

L. D. Cooley, X. Song, and D. C. Larbalestier

Applied Superconductivity Center, University of Wisconsin–Madison, 1500 Engineering Drive, Madison, Wisconsin 53706-1687

(Received 29 April 2002; accepted for publication 15 July 2002)

Bulk samples of MgB₂ were prepared with 5, 10, and 15 wt % Y₂O₃ nanoparticles, added using a simple solid-state reaction route. Transmission electron microscopy showed a fine nanostructure consisting of ~3–5 nm YB₄ nanoparticles embedded within MgB₂ grains of ~400 nm size. Compared to an undoped control sample, an improvement in the in-field critical current density J_C was observed, most notably for 10% doping. At 4.2 K, the lower bound J_C value was $\sim 2 \times 10^5$ A cm⁻² at 2 T. At 20 K, the corresponding value was $\sim 8 \times 10^4$ A cm⁻². Irreversibility fields were 11.5 T at 4.2 K and 5.5 T at 20 K. © 2002 American Institute of Physics. [DOI: 10.1063/1.1506184]

In slightly more than one year after the discovery of superconductivity in magnesium diboride, there is now a wide body of evidence indicating that MgB₂ does not contain intrinsic obstacles to current flow between grains, unlike the high-temperature superconducting cuprates. Evidence for strongly coupled grains has been found even in randomly aligned, porous, and impure samples,^{1,2} suggesting that dense forms of MgB₂ will be attractive in high-current applications at 20–30 K and perhaps 4.2 K. So far, however, bulk samples have demonstrated modest values of the irreversibility field $\mu_0 H^*(T)$ reaching about 4 T at 20 K and 8 T at 4.2 K.³ For comparison, established low-temperature superconductors, e.g., NbTi (10 T) and Nb₃Sn (20 T), have significantly higher irreversibility fields at 4.2 K, while Bi₂Sr₂Ca₂Cu₃O₁₀ (3 T) is becoming established at 20 K.⁴ MgB₂ tape results are somewhat more promising, with $\mu_0 H^*$ values of above 5 at 20 K,^{5–8} where partial orientation of crystallites parallel to the field is playing a role. Since the irreversibility field is the practical limit to magnet applications, it is desirable to make $\mu_0 H^*$ values as high as possible.

A central question is how to further increase the irreversibility field in addition to introducing crystallographic texture. Alloying additions, such as atomic substitution for Mg or B or added interstitial atoms, increase electron scattering and decrease the coherence length, producing higher upper critical and irreversibility fields.^{9,10} Adding nanometer-scale defects can produce similar effects. For example, proton irradiation studies showed that $\mu_0 H^*$ increased significantly from ~3.5 to ~6 T at 20 K with only moderate damage, corresponding to atomic displacements of a few %, due to either vacancies or interstitials.¹¹ Mechanical processing also produces structural defects, and similar increases in the irreversibility field have been reported.^{6,8,12} These increases

were steeper than the concomitant reductions in the critical temperature T_C , suggesting it is viable to improve the accessible field range without sacrificing other superconducting properties too much.

To explore more practical and scaleable routes to defect incorporation in bulk MgB₂, the present study explores chemical and nanostructural changes via addition of nanoparticles. Coherently ordered Mg–B–O precipitates are known to form in bulk MgB₂,¹³ thus suggesting MgO as an obvious second phase addition. However, we chose to study Y₂O₃ nanoparticle additions owing to the fact that nano-Y₂O₃ can be purchased cheaply and in large quantities. Cimberle *et al.*¹⁴ found that J_C increased by up to a factor of 3 for Li-, Al-, and Si-doped samples, although $\mu_0 H^*(T)$ remained unchanged at ~4 T for 20 K. Likewise, Feng and coworkers^{15,16} claimed much higher J_C for Ti- and Zr-doped samples at low fields.

In the present letter, we show that by the nanoparticle addition $\mu_0 H^*$ is increased to 11.5 T at 4.2 K and 5.5 T at 20 K, with an accompanying increase of J_C to $\sim 10^5$ A/cm² at 20 K, 2 T. A key finding is evidence for a regular distribution of YB₄ nanoprecipitates.

Doped samples were prepared from amorphous boron powder (99%, Fluka), 5, 10, or 15 wt % Y₂O₃ nanoparticles (15–30 nm particle size, 99.5%, Pi-Kem), and Mg powder (99%, Riedel-de Haen) by mixing and pressing into 5 mm diameter by 2 mm thick pellets. Undoped MgB₂ pellets were similarly prepared to the control samples. Reactions were performed at 900 °C in a reducing gas mixture of Ar–2% H₂. In order to counteract the effects of Mg loss, Mg foil was present in the reaction vessel during the reaction. The heating and cooling rates used were ~20 °C/min, and the dwell time at the peak temperature was 15 min.

The samples were clearly macroscopically porous when viewed by light microscopy (not shown). The geometrical densities for the different pellets were measured to be 50% ± 5%.

^{a)}Author to whom correspondence should be addressed; electronic mail: j.driscoll@ic.ac.uk

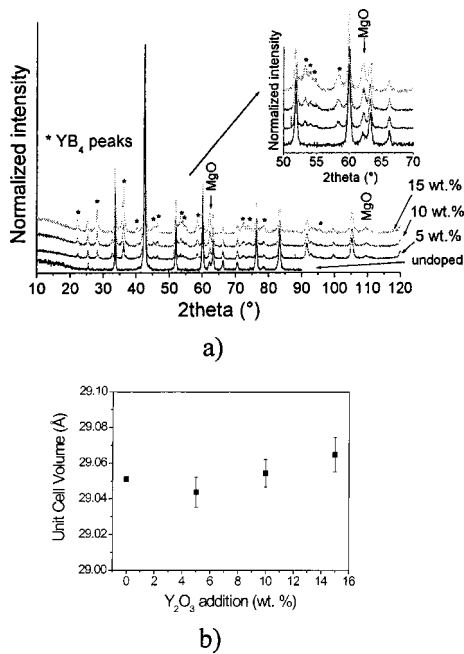


FIG. 1. X-ray diffraction of Y_2O_3 -doped MgB_2 . (a) Diffractograms of undoped, 5, 10, and 15 wt % Y_2O_3 -doped MgB_2 , and (b) volume of MgB_2 cell vs wt % Y_2O_3 .

Figure 1(a) shows the results of x-ray diffraction (XRD) analyses for the series of doped samples compared to an undoped sample. In addition to MgB_2 , small quantities of MgO and, in the doped samples, YB_4 , are indicated; there are no peaks corresponding to either pure Mg or Y_2O_3 . Hence, in the doped samples, it can be concluded that the Y_2O_3 reacted with B to form YB_4 . Since this decreased the amount of B available for reaction to MgB_2 , excess Mg either was transported away from the pellet or became oxidized. Indeed, an increase of the MgO peak intensities correlates with increasing Y_2O_3 fraction in Fig. 1(a). The volume of the MgB_2 unit cell was calculated as a function of Y_2O_3 fraction, which is shown in Fig. 1(b). The UnitCell program was used to refine the lattice parameters and calculate second phase particle sizes. There is possibly only a slight change in the unit cell volume with increased doping. This change might represent incorporation of oxygen into the lattice, or it could be due to strain from the added nanoparticles.

Figure 2(a) shows a transmission electron microscopy (TEM) diffraction contrast image of the 10% Y_2O_3 sample. The grain size of the MgB_2 is ~ 400 nm and precipitates at two different levels are seen. Precipitates with ~ 10 nm size occur at the MgB_2 grain boundaries (region 1), while inside the MgB_2 grain interior (region 2), evenly distributed, 3–5 nm precipitates are seen. A magnification of region 2 is shown in the inset of Fig. 2(a). Selected area diffraction patterns taken from both regions were very similar. Figure 2(b) shows the diffraction pattern along the MgB_2 [120] direction. The circled spots are consistent with MgB_2 and the indexed rings with YB_4 . Although all diffraction rings from MgO are contained in the more complex YB_4 pattern, additional rings were present for YB_4 , which could not be due to MgO , and therefore confirm that most of the precipitates are YB_4 . Large regions of MgO were observed in different areas of the sample and were found with 40–200 nm size. Diffraction

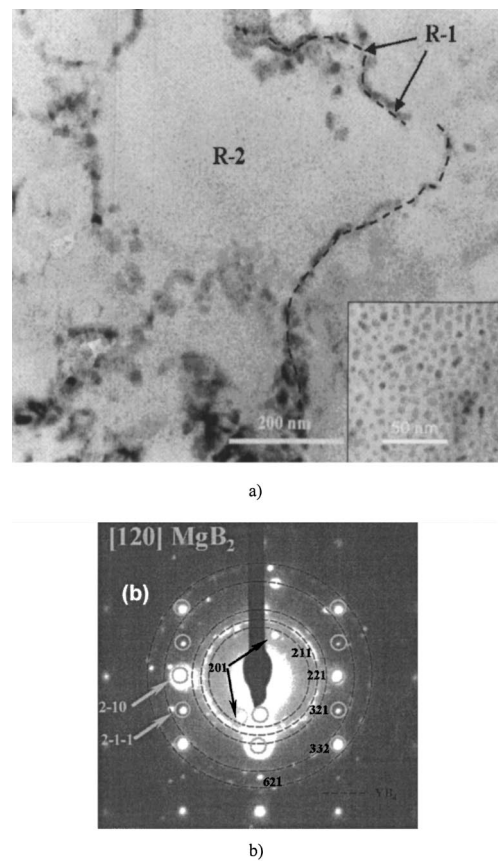


FIG. 2. TEM of 10 wt % Y_2O_3 -doped MgB_2 . (a) Micrograph showing nanoprecipitates of YB_4 embedded in MgB_2 grains, and (b) diffraction pattern along MgB_2 [120] direction. YB_4 ring pattern is outlined.

patterns confirm the MgO structure. However, YB_4 precipitates are also present within the MgO regions. The maximum particle sizes calculated from XRD for YB_4 and MgO were ~ 10 and ~ 150 nm, respectively, consistent with the TEM analyses.

Critical temperature T_c values were obtained by measuring the magnetic moment versus temperature $m(T)$ using a vibrating sample magnetometer (VSM), shown in Fig. 3. Samples were zero-field cooled and then warmed from 10 K in an applied field of 5 mT. Similar transitions, with an onset at ~ 39 K and an endpoint at ~ 38 K, are seen for the control, and the 5% and 10% Y_2O_3 samples, but these values are reduced by ~ 1 K for the 15% sample.

Figure 4 shows $J_c(H)$ at 20 K for the series of doped MgB_2 samples, as well as the undoped sample, a fragment of a sample from a commercial source, the 10 at. % Zr-doped sample of Feng *et al.*¹⁵ and high-pressure synthesized MgB_2 .¹⁷ The inset of Fig. 4 shows $J_c(H)$ at 4.2 K for the 10 wt. % Y_2O_3 doped sample. All samples were measured in a

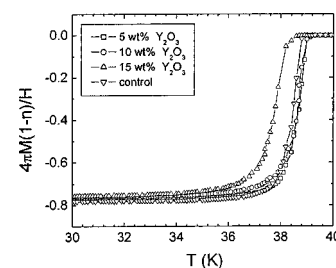


FIG. 3. Normalized dc magnetic susceptibility vs temperature for doped and undoped pellet samples. The demagnetization factors, n , were evaluated using the external sample dimensions.

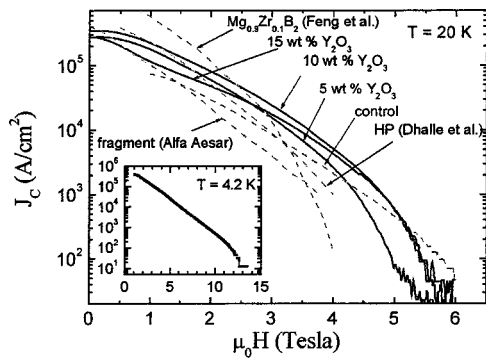


FIG. 4. $J_c(H)$ at 20 K for the series of Y_2O_3 -doped MgB_2 pellet samples, as well as an undoped pellet, a fragment of a sample from a commercial source (Alfa Aesar). For comparison, the 10 at. % Zr-doped sample of Feng *et al.* (Ref. 15) and high-pressure synthesized MgB_2 (Ref. 19) are included. Inset shows $J_c(H)$ at 4.2 K for the 10 wt % Y_2O_3 -doped sample.

VSM and the Bean model was used to deduce the critical current density from the magnetization hysteresis.¹⁸ For our measurements, in fields of <1 T the apparent plateau in J_c is artificial, due to saturation of the magnetometer. Therefore, the actual values are higher than shown. Our J_c values are based on full sample connectivity and are multiplied by 2 to allow for the 50% porosity. In fact, associated with the porosity is a reduction in the grain-to-grain contact area, and so a restriction of the cross section available for current flow. Also, the grain boundaries in the doped samples are partially obstructed by precipitates [Fig. 2(a)]. Consequently, these estimates are only lower bounds. Nonetheless, J_c is high and comparable to the fully dense, high-pressure synthesized material.¹⁹ The doping level of 10% produced the largest difference in both J_c and $\mu_0 H^*$. At 2 T, J_c for the sample is $\sim 8 \times 10^4$ A cm⁻², a factor of ~ 3 higher than for the undoped pellet sample and ~ 4 higher than the fragment. Compared to the Zr-doped sample, our low-field J_c values are lower in the ~ 1 –2 T region, but higher thereafter.

The $\mu_0 H^*$ value for the 10% Y_2O_3 -doped sample, as defined by a critical current density criterion of 10^2 A/cm², was 11.5 T at 4.2 K and 5.5 T at 20 K. The value at 20 K was confirmed to be 5.5 T from creep rate measurements (not shown), and is ~ 1.5 times higher than both the high-pressure and Zr-doped samples. The 4.2 K value is comparable with that for Nb–Ti. It is interesting that the control sample also has an enhanced irreversibility field, and this point is discussed further below.

The rapid formation technique used in this experiment apparently produced different superconducting properties, relative to those of high-pressure synthesized bulk, in all of the samples. However, at <4 T a higher irreversibility field and higher critical current density are seen for the doped samples, suggesting the additional effects of the nanoparticles. At >5 T, the undoped sample outperforms the doped samples, but this is most likely related to the greater connectivity of grain boundaries in the undoped sample, the doped samples having additional phases at the grain boundaries.

Interestingly, the samples show similar J_c and $\mu_0 H^*$ values to a recent report describing heavily ball milled, nanocrystalline powders of Gumbel *et al.*¹² However, ball milling also reduced T_c to 34.5 K, suggesting disorder or possibly alloying (from the milling process). Reduced T_c 's in the Zr-doped samples is also indicative of alloying.¹⁵ In the present

work, the critical temperature remains near 39 K, and there is a weak increase (if any) in the unit cell volume. We believe, therefore, that the nanoparticle additions neither alloyed the surrounding MgB_2 , nor produced significant disorder. The observed increase in $\mu_0 H^*$ may be due to increasing the number of point scattering sites, since the observed precipitates are 3–5 nm in size and uniformly distributed within the grains.

In summary, we have shown that incorporating Y_2O_3 nanoparticles together with Mg and B powders results in the formation of MgB_2 with a uniform dispersion of YB_4 nanoprecipitates. This nanostructure was achieved using a reaction at 900 °C for 15 min. The precipitates have 3–5 nm size, with larger ~ 10 nm precipitates occurring at some grain boundaries. At 20 K, the critical current density deduced by magnetization is $>10^5$ A/cm² in low fields, comparable to that of high-pressure synthesized bulk. Significant increases in the irreversibility field were also observed.

The work at Imperial College was supported by EPSRC and work at Wisconsin by the U.S. Department of Energy and the National Science Foundation.

¹D. K. Finnemore, J. E. Ostenson, S. L. Bud'ko, G. Lapertot, and P. C. Canfield, *Phys. Rev. Lett.* **86**, 2423 (2001).

²D. C. Larbalestier, M. Rikel, L. D. Cooley, A. A. Polyanskii, J. Y. Jiang, X. Y. Cai, D. M. Feldmann, A. Gurevich, A. A. Squitieri, M. T. Naus, C. B. Eom, E. E. Hellstrom, R. J. Cava, K. A. Regan, N. Rogado, A. Hayward, T. He, J. S. Slusky, P. Khalifah, I. Inumaru, and M. Haas, *Nature (London)* **410**, 186 (2001).

³C. Buzea and T. Yamashita, *Supercond. Sci. Technol.* **14**, R115 (2001).

⁴L. D. Cooley, C. B. Eom, E. E. Hellstrom, and D. C. Larbalestier, in *Proceedings of the 2001 Particle Accelerator Conference*, edited by P. Lucas and S. Webber (Institute of Electrical and Electronics Engineers, Piscataway, NJ, 2001), Vol. 1, pp. 203–207.

⁵S. H. Zhou, A. V. Pan, M. Ionescu, H. K. Liu, and S. X. Dou, *Supercond. Sci. Technol.* **15**, 236 (2002).

⁶H. L. Suo, C. Beneduce, M. Dhalle, N. Musolino, J. Y. Genoud, and R. Flukiger, *Appl. Phys. Lett.* **79**, 3116 (2001).

⁷A. K. Pradhan, Y. Feng, Y. Zhao, N. Koshizuka, L. Zhou, P. X. Zhang, X. H. Liu, P. Ji, S. J. Du, and C. F. Liu, *Appl. Phys. Lett.* **79**, 1649 (2001).

⁸C. Beneduce, H. L. Suo, P. Toulemonde, N. Musolino, and R. Flükiger, *cond-mat/0203551* (unpublished).

⁹C. B. Eom, M. K. Lee, J. H. Choi, L. Belenky, X. Song, L. D. Cooley, M. T. Naus, S. Patnaik, J. Jiang, M. Rikel, A. Polyanskii, A. Gurevich, X. Y. Cai, S. D. Bu, S. E. Babcock, E. E. Hellstrom, D. C. Larbalestier, N. Rogado, K. A. Regan, M. A. Hayward, T. He, J. S. Slusky, K. Inumaru, M. K. Haas, and R. J. Cava, *Nature (London)* **411**, 558 (2001).

¹⁰S. Patnaik, L. D. Cooley, A. Gurevich, A. A. Polyanskii, J. Jiang, X. Y. Cai, A. A. Squitieri, M. T. Naus, M. K. Lee, J. H. Choi, L. Belenky, S. D. Bu, J. Letteri, X. Song, D. G. Schlom, S. E. Babcock, C. B. Eom, E. E. Hellstrom, and D. C. Larbalestier, *Supercond. Sci. Technol.* **14**, 315 (2001).

¹¹Y. Bugoslavsky, L. F. Cohen, G. K. Perkins, M. Polichetti, T. J. Tate, R. G. William, and A. D. Caplin, *Nature (London)* **411**, 561 (2001).

¹²A. Gumbel, J. Eckert, G. Fuchs, K. Nenkov, K.-H. Müller, and L. Schultz, *Appl. Phys. Lett.* **80**, 2725 (2002).

¹³R. F. Klie, J. C. Idrobo, N. D. Browning, A. Serquis, Y. T. Zhu, X. Z. Liao, and F. M. Mueller, *Appl. Phys. Lett.* **80**, 3970 (2002).

¹⁴M. R. Cimberle, M. Novak, P. Manfrinetti, and A. Palenzona, *Supercond. Sci. Technol.* **15**, 34 (2002).

¹⁵Y. Feng, Y. Zhao, Y. P. Sun, F. C. Liu, Q. Fu, L. Zhou, C. H. Cheng, N. Koshizuka, and M. Murakami, *Appl. Phys. Lett.* **79**, 3983 (2001).

¹⁶Y. Zhao, Y. Feng, C. H. Cheng, L. Zhou, Y. Wu, T. Machi, Y. Fudamoto, N. Koshizuka, and M. Murakami, *Appl. Phys. Lett.* **79**, 1154 (2001).

¹⁷M. Dhalle, P. Toulemonde, C. Beneduce, N. Musolino, M. Decroux, and R. Flukiger, *Physica C* **363**, 155 (2001).

¹⁸C. P. Bean, *Rev. Mod. Phys.* **36**, 31 (1964).

¹⁹M. Dhalle, P. Toulemonde, C. Beneduce, N. Musolino, M. Decroux, and R. Flukiger, *Physica C* **363**, 155 (2001).